Journal of Applied Physics

On how to measure the probabilities of target atom ionization and target ion back-attraction in high-power impulse magnetron sputtering

Cite as: J. Appl. Phys. **129**, 033303 (2021); https://doi.org/10.1063/5.0036902
Submitted: 09 November 2020 . Accepted: 29 December 2020 . Published Online: 15 January 2021

Martin Rudolph, Hamidreza Hajihoseini, Michael A. Raadu, Jon Tomas Gudmundsson, Nils Brenning, Tiberiu M. Minea, André Anders, and Daniel Lundin

ARTICLES YOU MAY BE INTERESTED IN

Optimization of HiPIMS discharges: The selection of pulse power, pulse length, gas pressure, and magnetic field strength
Journal of Vacuum Science & Technology A **38**, 033008 (2020); https://doi.org/10.1116/6.0000079

High power impulse magnetron sputtering discharge
Journal of Vacuum Science & Technology A **30**, 030801 (2012); https://doi.org/10.1116/1.3691832

Sideways deposition rate and ionized flux fraction in dc and high power impulse magnetron sputtering
Journal of Vacuum Science & Technology A **38**, 033009 (2020); https://doi.org/10.1116/1.5145292

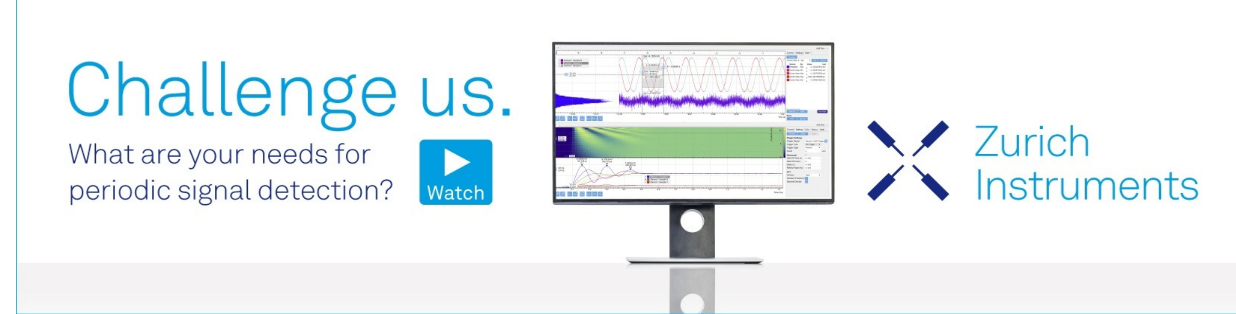

© 2021 Author(s).

Journal of Applied Physics ARTICLE scitation.org/journal/jap

On how to measure the probabilities of target atom ionization and target ion back-attraction in high-power impulse magnetron sputtering

Cite as: J. Appl. Phys. **129**, 033303 (2021); doi: 10.1063/5.0036902
Submitted: 9 November 2020 · Accepted: 29 December 2020 ·
Published Online: 15 January 2021

View Online

Export Citation

CrossMark

Martin Rudolph,[1,a)] Hamidreza Hajihoseini,[2,b)] Michael A. Raadu,[3] Jon Tomas Gudmundsson,[2,3] Nils Brenning,[3,4,5] Tiberiu M. Minea,[5] André Anders,[1,6] and Daniel Lundin[4,5]

AFFILIATIONS

[1]Leibniz Institute of Surface Engineering (IOM), Permoserstraße 15, 04318 Leipzig, Germany
[2]Science Institute, University of Iceland, Dunhaga 3, IS-107 Reykjavik, Iceland
[3]Department of Space and Plasma Physics, School of Electrical Engineering and Computer Science, KTH Royal Institute of Technology, SE-100 44 Stockholm, Sweden
[4]Plasma and Coatings Physics Division, IFM-Materials Physics, Linköping University, SE-581 83 Linköping, Sweden
[5]Laboratoire de Physique des Gaz et des Plasmas—LPGP, UMR 8578 CNRS, Université Paris–Sud, Université Paris–Saclay, 91405 Orsay Cedex, France
[6]Felix Bloch Institute of Solid State Physics, Leipzig University, Linnéstraße 5, 04103 Leipzig, Germany

[a)]**Author to whom correspondence should be addressed:** martin.rudolph@iom-leipzig.de
[b)]**Present address:** Industrial Focus Group XUV Optics, MESA+ Institute for Nanotechnology, University of Twente, Drienerlolaan 5, 7522 NB Enschede, The Netherlands.

ABSTRACT

High-power impulse magnetron sputtering (HiPIMS) is an ionized physical vapor deposition technique that provides a high flux of ionized target species for thin film growth. Optimization of HiPIMS processes is, however, often difficult, since the influence of external process parameters, such as working gas pressure, magnetic field strength, and pulse configuration, on the deposition process characteristics is not well understood. The reason is that these external parameters are only indirectly connected to the two key flux parameters, the deposition rate and ionized flux fraction, via two internal discharge parameters: the target atom ionization probability α_t and the target ion back-attraction probability β_t. Until now, it has been difficult to assess α_t and β_t without resorting to computational modeling, which has hampered knowledge-based optimization. Here, we present a simple method to deduce α_t and β_t based on measured deposition rates of neutrals and ions. The core of the method is a refined analytical model, which is described in detail. This approach is furthermore validated by independent calculations of α_t and β_t using the considerably more complex ionization region model, which is a plasma-chemical global discharge model.

Published under license by AIP Publishing. https://doi.org/10.1063/5.0036902

I. INTRODUCTION

High-power impulse magnetron sputtering (HiPIMS) is an ionized physical vapor deposition (IPVD) technique,[1] where magnetron sputtering[2] is merged with pulsed power technology.[3] In a HiPIMS discharge, high-power unipolar pulses are applied to the cathode target at a low duty cycle, while keeping the time-averaged power about two orders of magnitude lower than the peak power. This approach has been demonstrated to give improved properties of the deposited films, which has been related to high plasma density, and consequently a very high ionization fraction of the sputtered species.[4–6] The high ionization fraction of the sputtered species allows better control of the film growth as it makes it possible to control the energy and direction of the sputtered species and therefore the properties of the deposited film.[6] This is a significant advantage over dc magnetron sputtering (dcMS) where the film-forming material consists mainly of neutral species.[2]

Published under license by AIP Publishing.

A HiPIMS discharge can be tuned using a variety of different process parameters. External process parameters, such as the working gas pressure, the magnetic field strength, the degree of unbalance of the magnetron assembly, and the discharge current, are directly accessible to the operator. However, their influence on the deposition process often remains unclear, since they are only indirectly connected to two key flux parameters, the deposition rate and the ionized flux fraction,[7] which influence the production throughput and the quality of the deposited film.[6] The link between the external process parameters and the two flux parameters are two internal discharge parameters, the target atom ionization probability α_t and the target ion back-attraction probability β_t.[7] Knowledge of these two parameters allows us to estimate the deposition rate and the ionized flux fraction and therefore provides a quantitative insight into the quality of a deposition process and its efficiency.[7,8] More importantly, the understanding of how α_t and β_t change when changing external parameters is a key aspect for optimizing HiPIMS discharges.[7–9] Deducing α_t and β_t from simple measurements is, therefore, an important task. One approach is to use a quartz crystal microbalance (QCM), and from the measured deposition flux calculate the combined probability $\alpha_t\beta_t$ of ionized sputtered species back-attracted to the cathode target.[10] This was done by Bradley *et al.*[10] for discharges with different magnetic field strengths. They show that $\alpha_t\beta_t$ increases with increased magnetic field strength, thereby explaining the increased loss in deposition rate for stronger magnetic fields. However, an analysis by Brenning *et al.*[8] shows that small variations in $\alpha_t\beta_t$ may hide important and much larger individual changes of α_t and β_t in opposite directions and that these two parameters should be considered separately.

This approach was further developed by Hajihoseini *et al.*[11] who used a QCM-based ion meter (IM),[12] which allowed them to measure the deposited neutral and ion fluxes separately. They derived analytical expressions for α_t and β_t as functions of the two measured quantities. We herein call this analysis the "analytical model." It was used by Hajihoseini *et al.*[11] to analyze 11 discharges with varying magnetic field configurations. The authors identified a clear increase in α_t with increasing magnetic field strength and increasing peak discharge current when operating at a fixed discharge voltage. The variation in β_t, on the other hand, was less clear, but the data suggested an increasing trend with increasing magnetic field strength.[7,11] The combined trends in α_t and β_t were consistent with the earlier conclusions regarding the effect of magnetic field strength on $\alpha_t\beta_t$ by Bradley *et al.*[10] In addition to changing the magnetic field strength, Hajihoseini *et al.*[11] also varied the degree of magnetic balancing but were not able to pinpoint any trends in α_t and β_t due to large data scattering.

In this work, we refine the analytical model with the goal to provide a procedure on how to access α_t and β_t from simple measurements. The refined analytical model is furthermore validated by a plasma-chemical global discharge model, the ionization region model (IRM),[13,14] using the 11 discharges analyzed by Hajihoseini *et al.*[11] The paper is organized as follows. In Sec. II, we discuss the refinements made to the analytical model that gives α_t and β_t directly from measured deposition rates of neutrals and ions. These internal parameters are then independently determined by the IRM in Sec. III, and the results of the two models are compared. We summarize our findings in Sec. IV and outline the experimental procedure to deduce α_t and β_t from measurements without having to resort to computational modeling.

II. THEORY: A REFINED ANALYTICAL MODEL TO DERIVE α_t AND β_t

As a first step, we revise the analytical model of Hajihoseini *et al.*[11] and refine it in two aspects. First, we include the ratio of transport parameters for neutrals and ions $\xi_{tn}/\xi_{ti} \approx 2$ to take into account different scatter cones of neutrals and ions[15,16] as well as the influence of position and size of the substrate. ξ_t is the fraction of target species (subscript n = neutrals and i = ions) in the material flux from the ionization region (IR) to the diffusion region (DR) that is deposited on the substrate (located in the DR) and was first introduced by Vlček and Burcalová.[17] Second, we include a correction factor to compensate for the difference in scattering of target neutrals between dcMS and HiPIMS $\xi_{tn,HiPIMS}/\xi_{tn,dcMS}$.

A. Derivation of internal process parameters

We will in this sub-section derive expressions for estimating α_t and β_t based on two accessible quantities: (1) the sputter-rate-normalized deposition rate, which we denote $F^{IM}_{sput\to IM}$, and (2) the ionized flux fraction $F^{IM}_{ti,flux}$, which is defined below and calculated from measured deposition rates of neutrals and ions using the ion meter. For this task, we resort to the material pathways model.[17–19] It is an analytical model that describes the fate of the sputtered target material species in a magnetron sputtering discharge. It was used by Hajihoseini *et al.*[11] for their analytical approach to derive a relation between the measured quantities and α_t and β_t. Aspects of the material pathways model were also incorporated in the IRM,[20] so that all three models discussed in this work, namely, the analytical approach by Hajihoseini *et al.*,[11] the refinement of this approach in the present paper (i.e., the refined analytical model), and the IRM, all have the material pathways model as a common root.

Let us start with the overall picture of the fluxes of the film-forming material as shown in Fig. 1. The target material fluxes out of the ionization region to the diffusion region are denoted by Γ^{DR}_{tn} and Γ^{DR}_{ti} for target neutrals and target ions, respectively. Both quantities are already integrated over the surface of the IR and, therefore, are in units of particles per second. Only a part of this flux is deposited onto a substrate or onto an area of a flux-measuring device such as an ion meter. The fluxes onto the ion meter are indicated by a change in superscript to Γ^{IM}_{tn} and Γ^{IM}_{ti}. The fluxes are assumed to deposit onto the ion meter with an assumed sticking probability of one.

The fluxes out of the diffusion region and the fluxes onto the ion meter are related by the transport parameters ξ^{IM}_{tn} and ξ^{IM}_{ti} for neutrals and ions, respectively, and these are in general not equal.[21] There are several reasons for this, such as a larger scattering cross section for ions compared to neutrals[22] and ions, unlike neutrals, being influenced by the electric fields in the ionization region.[23] Also, plasma instabilities such as spokes with strong variations in magnitude and direction of the electric fields on short (typically microseconds) time scales further broaden the scatter cone of target ions.[24–27] The resulting angular distributions of neutrals and

Published under license by AIP Publishing.

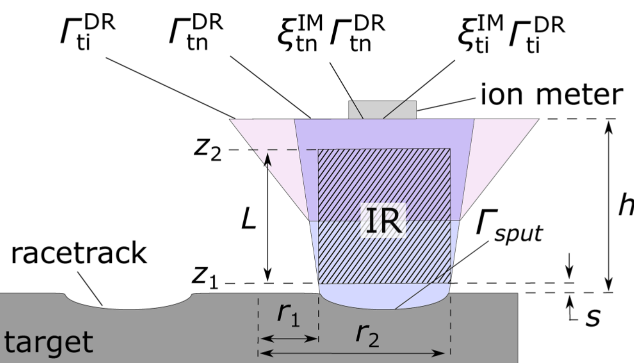

FIG. 1. A schematic showing the fluxes of the film-forming material from a section of the target racetrack and out of the ionization region. The dashed area indicates the volume of the ionization region bounded by r_1, r_2, z_1, and z_2. h denotes the perpendicular distance of the ion meter (IM) from the target and s is the cathode sheath thickness. The target fluxes Γ and transport parameters ξ are defined in the text. The schematic is not drawn to scale.

ions are schematically indicated by two scatter cones in Fig. 1. Keep in mind that this is a simplified sketch of the complex physics and that the fluxes are not homogeneously distributed over the bases of the cones. We are here not interested in the whole distributions but consider only the neutral and ion fluxes onto the ion meter. These fluxes are $\Gamma_{tn}^{IM} = f_{pulse}\xi_{tn}^{IM}\int_T \Gamma_{tn}^{DR}dt$ and $\Gamma_{ti}^{IM} = f_{pulse}\xi_{ti}^{IM}\int_T \Gamma_{ti}^{DR}dt$, respectively, where the integration is performed over one pulse period T, i.e., covering the pulse and the afterglow,[9] and then multiplied by the pulse frequency f_{pulse} in order to convert the fluxes to particles per second. In the following, we will only deal with fluxes onto the ion meter, and therefore, to simplify the expressions, we do not write out the superscripts on variables ξ_{tn}^{IM} and ξ_{ti}^{IM}, i.e., we use variables ξ_{tn} and ξ_{ti} instead.

To obtain the sputter rate-normalized deposition rate onto the ion meter $F_{sput\to IM}^{IM}$, the fluxes need to be normalized by a sputter rate. We here take the fraction of the sputtered flux Γ_{sput} that would be incident on the ion meter if the sputtered flux had remained neutral (i.e., was not reduced due to ionization) and had continued to the ion meter with unchanged transport parameter ξ_{tn}. We also use the approximation that there is negligible backscattering of sputtered neutral atoms back to the target. The latter approximation is similarly made in the material pathways model and in the IRM. For a purely neutral flux, this approximation corresponds to $\int_T \Gamma_{sput}\,dt = \int_T \Gamma_{tn}^{DR}dt$. We, thus, normalize the deposition rate by dividing the measured deposition on the ion meter, neutrals plus ions, with the neutral sputtered flux that "was on its way toward the IM" before it got depleted by ionization, i.e., by $\xi_{tn}\int_T \Gamma_{sput}dt$. Note that this approximation still includes scattering of the neutrals. A simple physical interpretation of this sputter-rate-normalized deposition rate is that it is a factor by which the deposition rate (neutrals plus ions) at the ion meter is increased to compensate for ionization followed by changes of the ion trajectories due to ion back-attraction and ion sideways transport. The sputter rate-normalized deposition rate then becomes

$$F_{sput\to IM}^{IM} = \frac{\xi_{tn}\int_T \Gamma_{tn}^{DR}dt + \xi_{ti}\int_T \Gamma_{ti}^{DR}dt}{\xi_{tn}\int_T \Gamma_{sput}\,dt} = \frac{\frac{\xi_{tn}}{\xi_{ti}}\int_T \Gamma_{tn}^{DR}dt + \int_T \Gamma_{ti}^{DR}dt}{\frac{\xi_{tn}}{\xi_{ti}}\int_T \Gamma_{sput}\,dt}. \tag{1}$$

The last step is a rewrite to replace the two separate variables ξ_{tn} and ξ_{ti} with their ratio ξ_{tn}/ξ_{ti}. They will appear together in this form in the equations to follow. As a side note, Γ_{sput} is easy to evaluate from a discharge model, such as the IRM. However, it is much more difficult to evaluate this quantity in an experimental discharge, which we will come back to in Sec. II B.

The ionized flux fraction $F_{ti,flux}^{IM}$ represents the share of the ion flux in the total flux of film-forming species deposited onto an IM. Also for this quantity, the individual neutral and ion fluxes Γ_{tn}^{DR} and Γ_{ti}^{DR} are normalized to the sputtered flux $\xi_{tn}\int_T \Gamma_{sput}dt$. As this sputtered flux appears in all terms, though, the normalization to $\xi_{tn}\int_T \Gamma_{sput}$ cancels out,

$$F_{ti,flux}^{IM} = \frac{\xi_{ti}\int_T \Gamma_{ti}^{DR}\,dt}{\xi_{tn}\int_T \Gamma_{tn}^{DR}\,dt + \xi_{ti}\int_T \Gamma_{ti}^{DR}\,dt} = \frac{\int_T \Gamma_{ti}^{DR}dt}{\frac{\xi_{tn}}{\xi_{ti}}\int_T \Gamma_{tn}^{DR}dt + \int_T \Gamma_{ti}^{DR}dt}. \tag{2}$$

With the explicit inclusion of the transport factors for neutrals ξ_{tn} and ions ξ_{ti}, Eq. (2) is a more general form of the equation for ionized flux fraction published by Hopwood[28] who assumed $\xi_{tn} = \xi_{ti}$.

The material fluxes $\int_T \Gamma_{sput}\,dt$ into the ionization region and $\int_T \Gamma_{tn}^{DR}dt$ and $\int_T \Gamma_{ti}^{DR}dt$ out of the ionization region to the diffusion region allow us to condense the complex discharge physics in the IR into the two parameters, α_t and β_t. The derivations make use of the conservation of the total number of particles that follows from the time-integrated particle fluxes,

$$\int_T \Gamma_{sput}\,dt = \int_T \Gamma_{tn}^{DR}\,dt + \int_T \Gamma_{ti}^{DR}\,dt + \int_T \Gamma_{ti}^{RT}\,dt. \tag{3}$$

Here, there is a term for the flux of ions of the sputtered target species back to the target that is taken to go only to the racetrack (hence the superscript RT). There is no net neutral flux onto the target due to the previous assumption of negligible backscattering of neutrals.

The target material ionization probability α_t describes the probability that a sputtered target neutral is ionized within the IR. It is given by the fraction of sputtered flux that does not leave the

Published under license by AIP Publishing.

IR as neutrals,[16]

$$\alpha_t = 1 - \frac{\int_T \Gamma_{tn}^{DR}\, dt}{\int_T \Gamma_{sput}\, dt}. \quad (4)$$

Similarly, the target ion back-attraction probability is given by the fraction of produced ions that do not leave the ionization region to the diffusion region,[16]

$$\beta_t = 1 - \frac{\int_T \Gamma_{ti}^{DR} dt}{\int_T \Gamma_{sput} dt - \int_T \Gamma_{tn}^{DR}\, dt}. \quad (5)$$

The sputter-rate-normalized deposition rate $F^{IM}_{sput\to IM}$ and the ionized flux fraction $F^{IM}_{ti,flux}$ can then be expressed as functions of the internal discharge parameters α_t and β_t by combining Eqs. (1), (2), (4), and (5) to give

$$F^{IM}_{sput\to IM} = (1-\alpha_t) + \left(\frac{\xi_{tn}}{\xi_{ti}}\right)^{-1} \alpha_t(1-\beta_t), \quad (6)$$

where ξ_{tn}/ξ_{ti} is evaluated at the position of the ion meter. For the special case $\xi_{ti} = \xi_{tn}$, this expression reduces to a reduction in the deposition rate by a factor $(1-\alpha_t\beta_t)$, in agreement with Bradley *et al.*[12] The ionized flux fraction at the substrate becomes

$$F^{IM}_{ti,flux} = \frac{1}{1 + \frac{\xi_{tn}}{\xi_{ti}} \times \frac{1-\alpha_t}{\alpha_t(1-\beta_t)}}. \quad (7)$$

A more general equation for the ionized flux fraction of the sputtered species was derived by Vlček and Burcalová.[17] Equation (7) describes the special case where no additional ionization of the sputtered species is assumed to occur in the diffusion region. This is safe to assume, as here we use experimental data recorded above the racetrack at the outer edge of the ionization region (see Fig. 1), which limits the effects of particle scattering in the diffusion region.

Reformulating Eqs. (6) and (7) yields α_t and β_t as functions of the sputter-rate-normalized deposition rate and the ionized flux fraction. The ionization probability of the sputtered species is then

$$\alpha_t = 1 - F^{IM}_{sput\to IM}(1 - F^{IM}_{ti,flux}). \quad (8)$$

The expression for the ion back-attraction probability β_t also follows from Eqs. (6) and (7),

$$\beta_t = \frac{F^{IM}_{sput\to IM} F^{IM}_{ti,flux}\left(1 - \frac{\xi_{tn}}{\xi_{ti}}\right) - F^{IM}_{sput\to IM} + 1}{1 - F^{IM}_{sput\to IM}(1 - F^{IM}_{ti,flux})}. \quad (9)$$

Equations (8) and (9) present a more general form of the equations for α_t and β_t than those given by Hajihoseini *et al.*[11] who assumed $\xi_{tn} = \xi_{ti}$. Also note that Eq. (9) can be rewritten so that only ion meter-related quantities derived from measurements appear on the right-hand side,

$$(1-\beta_t)\left(\frac{\xi_{tn}}{\xi_{ti}}\right)^{-1} = \frac{F^{IM}_{sput\to IM} F^{IM}_{ti,flux}}{1 - F^{IM}_{sput\to IM}(1 - F^{IM}_{ti,flux})}. \quad (10)$$

B. Deducing the flux parameters from measurements

To estimate the sputter-rate-normalized deposition rate and the ionized flux fraction, an ion meter can be used,[11,12] which is basically a charge-selective QCM. It is capable of determining the deposition rate of neutral film-forming species R^{IM}_{tn} (nm/min) and the deposition rate of ionized film-forming species R^{IM}_{ti} (nm/min). As the measure of the deposition rate from the ion meter is directly proportional to the fluxes $\xi_{tn}\int_T \Gamma^{DR}_{tn}$ and $\xi_{ti}\int_T \Gamma^{DR}_{ti}$, the readings from the ion meter (IM) can be readily used in Eq. (2) to obtain the ionized flux fraction,

$$F^{IM}_{ti,flux} = \frac{R^{IM}_{ti}}{R^{IM}_{ti} + R^{IM}_{tn}}. \quad (11)$$

For the sputter-rate-normalized deposition rate, the difficulty lies in determining the denominator in Eq. (1), $\xi_{tn}\int_T \Gamma_{sput} dt$. The neutral flux to the ion meter during the HiPIMS discharge is strongly reduced by ionization and ion back-attraction and is, thus, not proportional to the sputtered flux. One possibility would be to estimate the sputtered flux from the discharge current waveform, but this would yield the total flux and not the fraction of the flux which reaches the ion meter.

Here, we propose to use a slightly modified methodology to that proposed by Hajihoseini *et al.*[11] who estimated Γ_{sput} of the HiPIMS discharge using experimental data from a dcMS discharge operated at the same discharge power. We first extend the subscripts on parameters ξ and R^{IM} to clarify what discharge they refer to (HiPIMS or dcMS). Note that $\xi_{tn,HiPIMS} = \xi_{tn}$. The transport parameter ξ_{tn} appears in the ratio ξ_{tn}/ξ_{ti} which is introduced in Sec. II A. For the sake of clarity, we give the parameter a different subscript here, because in the following, it appears in a ratio together with $\xi_{tn,dcMS}$. The measured deposition rates on the ion meter are then $R^{IM}_{tn,dcMS}$, $R^{IM}_{tn,HiPIMS}$, and $R^{IM}_{ti,HiPIMS}$. Equation (1), with the same extended subscripts, then becomes

$$F^{IM}_{sput\to IM} = \frac{\xi_{tn,HiPIMS}\int_T \Gamma^{DR}_{tn,HiPIMS} dt + \xi_{sput,HiPIMS}\int_T \Gamma^{DR}_{ti,HiPIMS} dt}{\xi_{tn,HiPIMS}\int_T \Gamma_{sput,HiPIMS}\, dt}. \quad (12)$$

To relate the fluxes in Eq. (12) to measured deposition rates, we convert the involved expressions to a common unit. The measured output signals R^{IM} (in units of nm/min) from the ion meter are converted to particles per second by multiplying by a constant K_1, which we do not need to know since it will cancel out later. They are then converted to particles per pulse by division with the pulse frequency f_{pulse}. This gives for neutrals

$$\xi_{tn,HiPIMS}\int_T \Gamma^{DR}_{tn,HiPIMS} dt = \frac{K_1}{f_{pulse}} R^{IM}_{tn,HiPIMS}, \quad (13)$$

Published under license by AIP Publishing.

and for ions

$$\xi_{\mathrm{ti,HiPIMS}} \int_T \Gamma^{\mathrm{DR}}_{\mathrm{ti,HiPIMS}} dt = \frac{K_1}{f_{\mathrm{pulse}}} R^{\mathrm{IM}}_{\mathrm{ti,HiPIMS}}. \tag{14}$$

In the dcMS case, the deposition rate (here, in particles per second) can be expressed in three different ways as

$$\xi_{\mathrm{tn,dcMS}} \Gamma^{\mathrm{DR}}_{\mathrm{tn,dcMS}} = \xi_{\mathrm{tn,dcMS}} \Gamma_{\mathrm{sput,dcMS}} = K_1 R^{\mathrm{IM}}_{\mathrm{tn,dcMS}}. \tag{15}$$

For the first step, we assume that all sputtered species enter the DR and $\Gamma^{\mathrm{DR}}_{\mathrm{tn,dcMS}} = \Gamma_{\mathrm{sput,dcMS}}$, which follows from the assumptions of negligible ionization of the sputtered species in dcMS, and that no sputtered neutrals return to the target.

In the denominator in Eq. (12), we replace $\int_T \Gamma_{\mathrm{sput,HiPIMS}} dt$ with $\Gamma_{\mathrm{sput,HiPIMS}}/f_{\mathrm{pulse}}$, where $\Gamma_{\mathrm{sput,HiPIMS}}$ is the time-averaged sputter rate in HiPIMS, and rewrite the resulting expression by multiplying through with $\xi_{\mathrm{tn,dcMS}}/\xi_{\mathrm{tn,dcMS}}$ and $\Gamma_{\mathrm{sput,dcMS}}/\Gamma_{\mathrm{sput,dcMS}}$,

$$\begin{aligned}\xi_{\mathrm{tn,HiPIMS}} \int_T \Gamma_{\mathrm{sput,HiPIMS}}\, dt &= \frac{\xi_{\mathrm{tn,HiPIMS}} \Gamma_{\mathrm{sput,HiPIMS}}}{f_{\mathrm{pulse}}} \\ &= \xi_{\mathrm{tn,dcMS}} \frac{\xi_{\mathrm{tn,HiPIMS}}}{\xi_{\mathrm{tn,dcMS}}} \frac{\Gamma_{\mathrm{sput,dcMS}} \dfrac{\Gamma_{\mathrm{sput,HiPIMS}}}{\Gamma_{\mathrm{sput,dcMS}}}}{f_{\mathrm{pulse}}}.\end{aligned} \tag{16}$$

The product $\xi_{\mathrm{tn,dcMS}}\Gamma_{\mathrm{sput,dcMS}}$ is then rewritten as $K_1 R^{\mathrm{IM}}_{\mathrm{tn,dcMS}}$ using Eq. (15), and we obtain

$$\xi_{\mathrm{tn,HiPIMS}} \int_T \Gamma_{\mathrm{sput,HiPIMS}}\, dt = \frac{K_1}{f_{\mathrm{pulse}}} R^{\mathrm{IM}}_{\mathrm{tn,dcMS}} \frac{\xi_{\mathrm{tn,HiPIMS}}}{\xi_{\mathrm{tn,dcMS}}} \frac{\Gamma_{\mathrm{sput,HiPIMS}}}{\Gamma_{\mathrm{sput,dcMS}}}. \tag{17}$$

Replacing the expressions in Eq. (12) with the expressions in Eqs. (13), (14), and (17), we obtain (after cancelling the factors K_1/f_{pulse})

$$F^{\mathrm{IM}}_{\mathrm{sput}\to\mathrm{IM}} = \frac{R^{\mathrm{IM}}_{\mathrm{tn,HiPIMS}} + R^{\mathrm{IM}}_{\mathrm{ti,HiPIMS}}}{R^{\mathrm{IM}}_{\mathrm{tn,dcMS}} \dfrac{\xi_{\mathrm{tn,HiPIMS}}}{\xi_{\mathrm{tn,dcMS}}} \times \dfrac{\Gamma_{\mathrm{sput,HiPIMS}}}{\Gamma_{\mathrm{sput,dcMS}}}}. \tag{18}$$

This is the sought relation. To evaluate the sputter-rate-normalized deposition rate from the measured values, we need the two ratios to the right in the denominator. The rightmost ratio accounts for the difference in the power-normalized sputter rates between HiPIMS and dcMS. Hajihoseini *et al.*[11] denote this quantity as Ψ and give the expression

$$\frac{\Gamma_{\mathrm{sput,HiPIMS}}}{\Gamma_{\mathrm{sput,dcMS}}} \equiv \Psi = \frac{V_{\mathrm{D,dcMS}}}{V_{\mathrm{D,HiPIMS}}} \times \frac{\zeta Y_{\mathrm{tg}}(V_{\mathrm{D,HiPIMS}}) + (1-\zeta) Y_{\mathrm{SS}}(V_{\mathrm{D,HiPIMS}})}{Y_{\mathrm{tg}}(V_{\mathrm{D,dcMS}})}, \tag{19}$$

which corrects for the fact that the sputter yield depends on the ion energy and the ion type. Here, $V_{\mathrm{D,dcMS}}$ and $V_{\mathrm{D,HiPIMS}}$ are the cathode potentials for the dcMS and the HiPIMS discharge, respectively; ζ and $(1-\zeta)$ are the fractions of the ion currents to the cathode carried by Ar^+ and Ti^+ ions, respectively; and $Y_{\mathrm{tg}}(V_{\mathrm{D}})$ and $Y_{\mathrm{SS}}(V_{\mathrm{D}})$ are the sputter yields as functions of the applied discharge voltage for Ar^+ and Ti^+ ions, respectively. Hajihoseini *et al.*[11] estimate that, for the studied HiPIMS discharge, typically half the discharge current is carried by Ar^+ ions, the other half by Ti^+ ions, and that there is a negligible contribution from secondary electrons and doubly charged ions. This is an estimate based on the concept of critical discharge current[14,29] which thus gives $\zeta \approx 1-\zeta \approx 0.5$. Using empirical formulas for the sputter yield from Anders *et al.*,[30] Eq. (19) gives Ψ in the range 0.61–0.71 depending on the ion composition (ζ) and a value $\Psi = 0.66$ is taken for $\zeta = 0.5$ for all discharges investigated.[11]

The remaining factor $\xi_{\mathrm{tn,HiPIMS}}/\xi_{\mathrm{tn,dcMS}}$ in Eq. (18) was assumed to be close to 1 by Hajihoseini *et al.*[11] This is where the refined analytical model differs. There is larger gas rarefaction in HiPIMS, mainly due to ionization losses during the pulses[31] as well as a higher working gas temperature with increasing peak currents.[32] In our measurements, the ion meter is placed above the racetrack center, presumably right in the most intense sputtered flux. Elastic collisions between sputtered neutrals and Ar atoms will spread the sputtered beam and therefore reduce ξ_{tn} for this particular location. The lower working gas density within the IR of a HiPIMS discharge gives less such scattering and therefore a value of $\xi_{\mathrm{tn,HiPIMS}}/\xi_{\mathrm{tn,dcMS}}$ above 1. A realistic estimate is, however, very difficult to make. We instead turn the problem the other way around. Testing the refined analytical model with different values of $\xi_{\mathrm{tn,HiPIMS}}/\xi_{\mathrm{tn,dcMS}}$, we find that a value of $\approx$1.9 gives the best overall agreement with the IRM calculations discussed in Sec. III, and this value will be used herein. The factor $\xi_{\mathrm{tn,HiPIMS}}/\xi_{\mathrm{tn,dcMS}} \approx 1.9$ can be partially justified by simple estimates involving the difference in Ar gas temperature that influences the mean free path $\lambda_{\mathrm{mfp}} = 1/n(T_{\mathrm{gas}})\sigma_{\mathrm{ArTi}}$ of the sputtered Ti neutrals. $n(T_{\mathrm{gas}})$ is the temperature-dependent working gas density calculated from the ideal gas law, and σ_{ArTi} is the scattering cross section between Ti and Ar neutrals. For the dcMS discharge, we note that a fraction $1-\exp(-h/\lambda_{\mathrm{mfp,dcMS}})$ of target neutrals are scattered out of their trajectory toward the ion meter, where h is the distance between the target and the ion meter (Fig. 1). For this study, $h = 30$ mm. Thus, without any scattering, the flux would be a factor $1/\exp(-h/\lambda_{\mathrm{mfp,dcMS}})$ higher. In the HiPIMS case, the flux is reduced by a factor $\exp(-h/\lambda_{\mathrm{mfp,HiPIMS}})$. This gives

$$\frac{\xi_{\mathrm{tn,HiPIMS}}}{\xi_{\mathrm{tn,dcMS}}} \approx \frac{\exp\left(-\dfrac{h}{\lambda_{\mathrm{mfp,HiPIMS}}}\right)}{\exp\left(-\dfrac{h}{\lambda_{\mathrm{mfp,dcMS}}}\right)}. \tag{20}$$

Using an Ar working gas pressure $p = 1$ Pa, a scattering cross section $\sigma_{\mathrm{ArTi}} \approx 2\times10^{-19}\,\mathrm{m}^2$,[14,33] the distance to the QCM $h = 30$ mm (Fig. 1) and a gas temperature in the HiPIMS case of $T_{\mathrm{gas,HiPIMS}} = 500$ K[32] and the dcMS case of $T_{\mathrm{gas,dcMS}} = 300$ K, we

Published under license by AIP Publishing.

calculate $\xi_{tn,HiPIMS}/\xi_{tn,dcMS} = 1.8$. Additional gas rarefaction due to ionization losses in the HiPIMS case[31] will add to this factor. For the practical application of this model, we recommend to make a similar estimate for the gas temperatures between dcMS and HiPIMS. An uncertain value of $\xi_{tn,HiPIMS}/\xi_{tn,dcMS}$ will naturally propagate down to the values of α_t and β_t. An estimate on the uncertainty bars for α_t and β_t based on the errors made in estimating $\xi_{tn,HiPIMS}/\xi_{tn,dcMS}$ is given in Appendix.

III. RESULTS AND DISCUSSION

A. Comparison of analytical and refined analytical models

Here, we reuse data from the study by Hajihoseini *et al.*[11] to compare the results of the analytical model from this publication, with the results of our refined analytical model. In this work, the authors studied HiPIMS discharges with a 4″ Ti target, 6 mm in thickness, in Ar working gas for a range of magnetic field configurations. The magnetron assembly had a central (C) and an annular edge (E) magnet that could individually be moved away from the rear surface of the target. The different magnetic configurations were termed C*x*E*y*, where *x* and *y* denoted the distance in millimeter of each magnet to the position closest to the rear surface of the target. For each magnetic configuration, the magnetron sputtering discharge was operated in two different modes: (1) Fixed current mode, where the peak discharge current amplitude was kept constant at $I_{D,peak} \approx 40$ A ($J_{D,peak} \approx 0.5$ A/cm^2 averaged over the target surface), and (2) fixed voltage mode, where the discharge voltage during the pulse was kept constant at $V_D \approx 625$ V. From these discharges, they recorded deposition rates R_{tn}^{IM} and R_{ti}^{IM} for neutrals and ions, respectively, using an ion meter[12] that was positioned at an axial distance of $h = 30$ mm and 70 mm above the racetrack.[11] In order to calculate α_t and β_t, Hajihoseini *et al.*[11] also recorded corresponding rates from a dcMS discharge operated at the same average power (see also Sec. II B). Here, we use the experimental dataset recorded at $h = 30$ mm above the racetrack (see Fig. 1) instead of the measurements made at $h = 70$ mm, which were used in Hajihoseini *et al.*[11] The reason is that validation of calculated α_t and β_t values using the IRM (Sec. III B) requires measuring R_{tn}^{IM} and R_{ti}^{IM} close to the edge of the ionization region to limit additional scattering of the flux in the diffusion region.

The ionized flux fraction $F_{ti,flux}^{IM}$ can be readily calculated using the measured ion and neutral deposition rates according to Eq. (11). The sputter-normalized deposition rate $F_{sput\to IM}^{IM}$ is calculated according to Eq. (18), which requires knowledge of the power-normalized sputter rates between HiPIMS and dcMS, $\Psi = \Gamma_{sput,HiPIMS}/\Gamma_{sput,dcMS}$, defined in Eq. (19) as well as the factor $\xi_{tn,HiPIMS}/\xi_{tn,dcMS}$. Based on the discussion in Sec. II B, we use $\Psi = 0.66$ and $\xi_{tn,HiPIMS}/\xi_{tn,dcMS} = 1.9$ for all discharges investigated. The resulting values of $F_{sput\to IM}^{IM}$ and $F_{ti,flux}^{IM}$ are given in Table I for all magnetic field configurations investigated. From these values, it is straightforward to calculate α_t and β_t using Eqs. (8) and (9), which are also given in Table I.

A comparison between the internal discharge parameters α_t and β_t using our refined analytical model and the analytical model from Hajihoseini *et al.*[11] with data obtained at $h = 30$ mm above the racetrack from the same publication shows quite some differences (Fig. 2). For α_t, the two models are positively correlated in the sense that a larger α_t in one model also gives a larger α_t in the other. However, the refined analytical model always gives larger values for α_t compared to the analytical model [Fig. 2(a)]. For β_t, it is difficult to judge on the correlations. For the fixed current mode discharges, the positive correlation is conserved. For the fixed voltage discharges, the refined analytical model gives little variation in β_t while the analytical model gives a large spread [Fig. 2(b)]. For both types of discharge modes, the refined analytical model gives values of β_t that are larger compared to the analytical model. The higher values of α_t and β_t can be traced back to the introduction of the ratio $\xi_{tn,HiPIMS}/\xi_{tn,dcMS}$. This factor decreases the value of $F_{sput\to IM}^{IM}$ in Eq. (18), which subsequently increases the value of α_t

TABLE I. Measured total (R_{tot}^{IM}), neutral (R_{tn}^{IM}), and ion deposition rates ($R_{ti}^{IM} = R_{tot}^{IM} - R_{tn}^{IM}$), and calculated flux as well as internal discharge parameters from the refined analytical model. The measured rates are extracted from the work of Hajihoseini *et al.*,[11] where also detailed mapping of the different magnetic field configurations is given.

		Measured rates from an ion meter			Calculated parameters using the refined analytical model			
	Magnetic configuration	R_{tot}^{IM} (nm/min)	R_{tn}^{IM} (nm/min)	$R_{tot,dcMS}^{IM}$ (nm/min)	$F_{sput\to IM}^{IM}$	$F_{ti,flux}^{IM}$	α_t	β_t
Fixed current mode	C0E0	25.2	20.8	70.6	0.28	0.17	0.77	0.87
	C0E5	27.6	23.6	74.2	0.30	0.14	0.75	0.88
	C0E10	29.6	25.0	69.7	0.34	0.16	0.71	0.85
	C5E0	27.6	22.0	69.7	0.32	0.20	0.75	0.83
	C5E5	26.0	21.6	69.7	0.30	0.17	0.75	0.87
	C10E0	24.8	20.6	62.3	0.32	0.17	0.74	0.85
Fixed voltage mode	C0E0	20.6	14.4	70.6	0.23	0.30	0.84	0.83
	C0E5	25.4	20.8	74.2	0.27	0.18	0.78	0.87
	C0E10	33.8	28.6	69.7	0.39	0.15	0.67	0.82
	C5E0	24.6	20.0	69.7	0.28	0.19	0.77	0.86
	C5E5	32.4	28.0	69.7	0.37	0.14	0.68	0.85
	C10E0	33.0	28.8	62.3	0.42	0.13	0.63	0.83
	C10E10	50.5	48.0	69.7	0.58	0.05	0.45	0.87

Published under license by AIP Publishing.

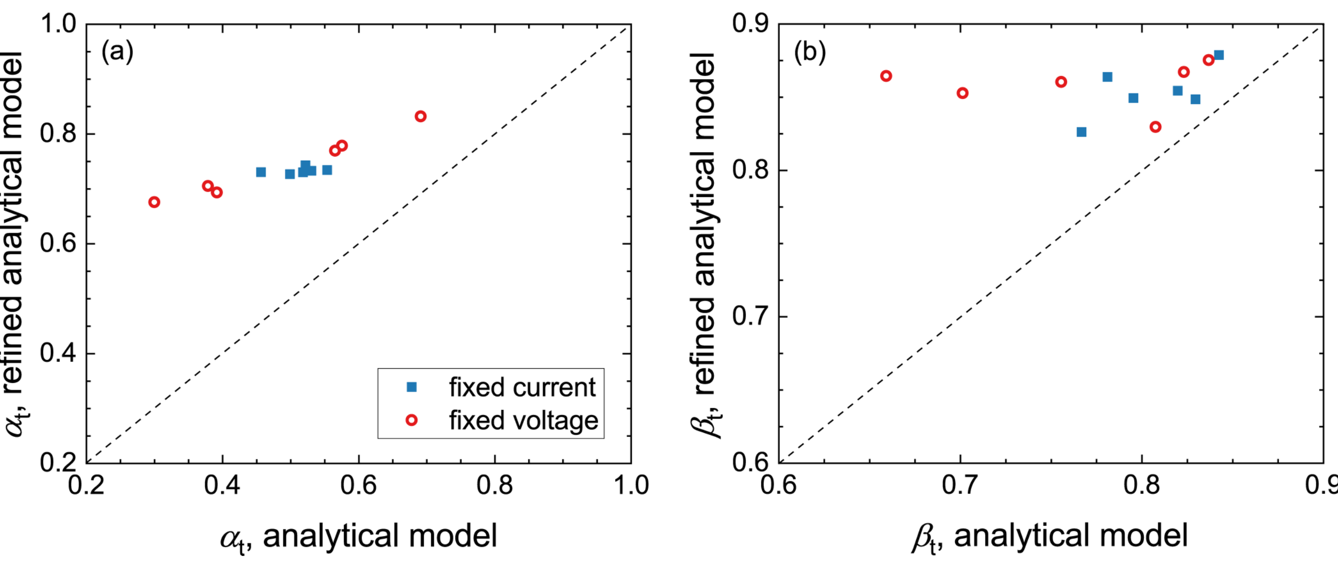

FIG. 2. Comparison between the analytical model from Hajihoseini *et al.*[11] and the refined model derived in this work using the dataset recorded at h = 30 mm above the racetrack.[11] The dashed line is a straight line through the origin with a slope of 1.

in Eq. (8). The same reason applies to the differences in β_t. The lower value of $F^{IM}_{sput\rightarrow IM}$ in Eq. (10) decreases the value of the left-hand side containing $(1-\beta_t)$, which consequently gives a higher value of β_t. This shows the importance of considering the difference in target atom scattering in the IR between dcMS and HiPIMS discharges.

B. Validating the refined analytical model using the ionization region model (IRM)

The results of the refined analytical model are here validated using the IRM, which is a global volume averaged plasma-chemistry model based on particle and power balance.[13,14] We use the version of the IRM that includes the consideration of an afterglow, which is important to account for, since the contribution to the deposition rate of the afterglow can be a significant portion of the total deposition rate,[9] which has been verified experimentally.[34] Furthermore, we introduce the explicit treatment of two separate Ar metastable levels ($^3P_2$ at 11.548 eV and $^3P_0$ at 11.723 eV). These changes include an update of the corresponding forward and backward electron impact excitation cross sections to and from the metastable levels and a new ionization cross section from these metastable levels. The details of the revised rate coefficients are published elsewhere.[35]

The model is fitted according to a well-described procedure (see Refs. 14 and 16) using the measured ionized flux fraction and the measured discharge current and voltage waveforms. The IR volume in the IRM model is assumed to be defined by $r_1 = 11$ mm, $r_2 = 39$ mm, $z_1 = 2$ mm, and $z_2 = 25$ mm. The resulting fitting parameters for the fractional drop of the cathode voltage over the IR, $f = V_{IR}/V_D$, and the target ion back-attraction probability during the pulse, $\beta_{t,pulse}$, are summarized in Table II. The recapture probability of secondary electrons due to the effect of the magnetic field on the electron trajectories is assumed to be 0.7 for all discharges investigated.[9]

From the IRM output, $\alpha_{t,IRM}$ can be calculated from the Ti ionization rate $r_{t,ion}$ (in s^{-1}) and the Ti sputter rate Γ_{sput} according to

TABLE II. IRM fitting parameters, the fractional drop of cathode voltage over the ionization region ($f = V_{IR}/V_D$), and the target ion back-attraction probability during the pulse ($\beta_{t,pulse}$) together with the model-derived internal discharge parameters $\alpha_{t,IRM}$ and $\beta_{t,IRM}$.

	Magnetic configuration	IRM fitting parameters		IRM-derived internal discharge parameters	
		$f = V_{IR}/V_D$	$\beta_{t,pulse}$	$\alpha_{t,IRM}$	$\beta_{t,IRM}$
Fixed current	C0E0	0.099	0.89	0.73	0.85
	C0E5	0.086	0.92	0.73	0.88
	C0E10	0.069	0.90	0.73	0.86
	C5E0	0.090	0.87	0.74	0.83
	C5E5	0.064	0.90	0.73	0.85
	C10E0	0.062	0.89	0.73	0.85
Fixed voltage	C0E0	0.071	0.87	0.83	0.83
	C0E5	0.064	0.92	0.78	0.88
	C0E10	0.065	0.89	0.71	0.85
	C5E0	0.065	0.91	0.77	0.87
	C5E5	0.064	0.91	0.69	0.86
	C10E0	0.063	0.91	0.68	0.86
	C10E10	0.059	0.93	0.45	0.86

Published under license by AIP Publishing.

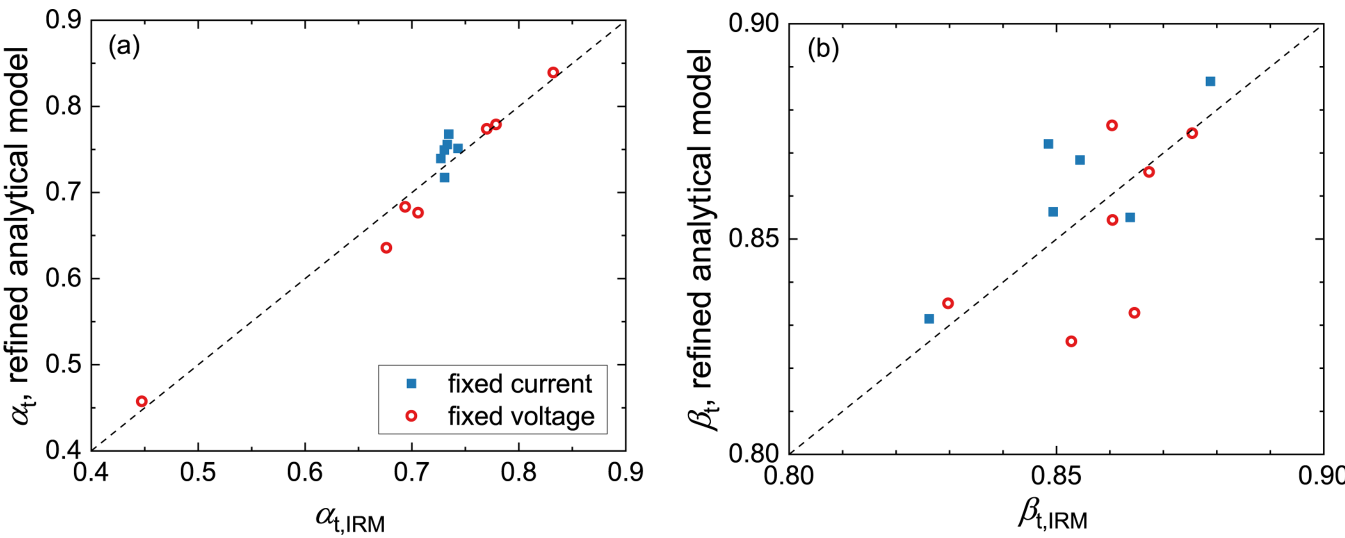

FIG. 3. Comparison of the internal discharge parameters (a) α_t and (b) β_t from the refined analytical model and the global plasma-chemical discharge model IRM. The dashed line is a straight line through the origin with a slope of 1. Note that the axes in panel (b) are truncated at 0.8 and 0.9. This exaggerates the data scattering.

$$\alpha_{t,IRM} = \frac{\int_T r_{t,ion} dt}{\int_T \Gamma_{sput} dt}. \tag{21}$$

To be consistent with the experimental measurements, for which no distinction is made between Ti^+ and Ti^{2+} ions, we consider only the electron impact ionization rate from neutral Ti to Ti^+ for the calculation of α_t. In the IRM, Ti^{2+} is produced from singly ionized Ti^+ only. Thus, the doubly charged ions are treated in the calculation of α_t as if they were Ti^+ ions. $\beta_{t,IRM}$ is calculated from the ion fluxes to the racetrack (RT) for singly and doubly ionized Ti, Γ_{ti}^{RT}, and the fluxes of single and doubly ionized Ti to the diffusion region (DR), Γ_{ti}^{DR}, respectively,

$$\beta_{t,IRM} = \frac{\int_T \Gamma_{ti}^{RT} dt}{\int_T (\Gamma_{ti}^{RT} + \Gamma_{ti}^{DR})\, dt}. \tag{22}$$

The IRM-derived parameters $\alpha_{t,IRM}$ and $\beta_{t,IRM}$ are summarized in Table II. A comparison between the internal discharge parameters from the numerical and analytical models is presented in Fig. 3. The trends of α_t and β_t given by the refined analytical model match perfectly with the trends given by the IRM. Also, the absolute values match quite well between the two approaches. The comparison of absolute values in Fig. 3 shows that α_t and β_t can be determined with good precision using the refined analytical model. Note that due to the limited spread in the values of β_t,[7,16] the data points in Fig. 3 are clustered at around 0.85. This does not mean that changes of this value are irrelevant as small changes in β_t can still have large effects on the flux parameters $F_{sput\to IM}^{IM}$ and $F_{ti,flux}^{IM}$. This is seen in Eqs. (6) and (7), which both contain a term $(1-\beta_t)$ that naturally has a much larger relative range compared to β_t.[7] It is, therefore, important to determine β_t with high precision. It is also important to note that too small variations in the value of β_t between two discharges may be covered by data scattering seen in Fig. 3(b).

IV. SUMMARY

High-power impulse magnetron sputtering discharges often exhibit complex discharge physics in the ionization region close to the cathode target, which makes optimization challenging. The reason is that external parameters, such as working gas pressure, magnetic field strength, and pulse configuration, are only indirectly connected to the two key flux parameters: deposition rate and ionized flux fraction. The link between the external process parameters and the two flux parameters are two internal discharge parameters, the target atom ionization probability α_t and the target ion back-attraction probability β_t, which have so far been difficult to assess without resorting to computational modeling. In the present work, we present a simple method to deduce α_t and β_t based on measured deposition rates of neutrals and ions. The procedure available to the operator is summarized as follows:

- The total deposition rate R_{tot}^{IM} and the deposition rate due to neutrals only R_{tn}^{IM} need to be measured for the desired HiPIMS discharge from which the deposition rate of ions can be deduced as $R_{ti}^{IM} = R_{tot}^{IM} - R_{tn}^{IM}$. The total deposition rate in dcMS $R_{tot,dcMS}^{IM}$ at the same average power is also required. These measurements can be realized using, for example, a gridded QCM or an ion meter, as described in Sec. I. It is recommended to carry out the measurements above the racetrack at the outer edge of the ionization region (see Fig. 1), i.e., close to the magnetic trap, since this limits the effects of particle scattering in the diffusion region, where the substrate is typically located.
- Using the acquired rates, it is straightforward to calculate the ionized flux fraction $F_{ti,flux}^{IM}$ from Eq. (11). The sputter-rate-

Published under license by AIP Publishing.

normalized deposition rate $F^{IM}_{sput\to IM}$ is calculated from Eq. (18) using the same deposition rates, which also requires evaluating the difference in the power-normalized sputter rates, denoted as Ψ [Eq. (19)], and the ratio $\xi_{tn,HiPIMS}/\xi_{tn,dcMS}$, which accounts for changes in elastic scattering due to strong gas rarefaction in HiPIMS. Suitable values are $\Psi = 0.66$ and $\xi_{tn,HiPIMS}/\xi_{tn,dcMS} = 1.9$ and are discussed in detail in Sec. II B. Please note that the former value applies to the case studied here: a Ti/Ar discharge with a typical peak discharge current density around 0.5 A/cm^2, and that Ψ has to be re-evaluated for other parameter combinations as it depends on sputter yields and discharge voltages.

- Using the calculated values of $F^{IM}_{ti,flux}$ and $F^{IM}_{sput\to IM}$, α_t and β_t can now be deduced directly from Eqs. (8) and (9), respectively. Calculating β_t requires evaluating the ratio of transport parameters ξ_{tn}/ξ_{ti}, which takes into account that fluxes of neutrals and ions onto the ion meter are generally not equal and typically closer to $\xi_{tn}/\xi_{ti} \approx 2$, as discussed by Butler *et al.*[16]

The above procedure is furthermore validated by independent calculations of α_t and β_t using the considerably more complex ionization region model (IRM), which is numerically solved. The good agreement makes the proposed solution a suitable tool for process developers to access the internal discharge parameters and will hopefully contribute to accelerating research and development in HiPIMS processes by providing an alternative to empirical approaches.

ACKNOWLEDGMENTS

This work was partially funded by the Free State of Saxony and the European Regional Development Fund (Grant No. 100336119), the Icelandic Research Fund (Grant Nos. 130029 and 196141), the Swedish Research Council (Grant No. VR 2018-04139), and the Swedish Government Strategic Research Area in Materials Science on Functional Materials at Linköping University (Faculty Grant SFO-Mat-LiU No. 2009-00971).

APPENDIX: UNCERTAINTY ANALYSIS FOR α_t AND β_t.

The refined analytical model contains two quantities for which no established method exists to determine them. These are the ratio of transport parameters between neutrals and ions in a HiPIMS discharge, ξ_{tn}/ξ_{ti}, and the ratio of transport parameters between a HiPIMS and a dcMS discharge at equal average power, $\xi_{tn,HiPIMS}/\xi_{tn,dcMS}$. In the following, we estimate to what extent uncertainties in these ratios affect α_t and β_t.

We start with the ratio ξ_{tn}/ξ_{ti}. Equation (8) shows that α_t is independent of the ratio ξ_{tn}/ξ_{ti}. For β_t, we note that the parameter $(1-\beta_t)$ is linearly proportional to ξ_{tn}/ξ_{ti} [Eq. (10)]. Therefore, the fractional uncertainty in $(1-\beta_t)$, i.e., $\delta(1-\beta_t)/(1-\beta_t)$, is equal to fractional uncertainty in $\delta(\xi_{tn}/\xi_{ti})/(\xi_{tn}/\xi_{ti})$, i.e., a fractional uncertainty in (ξ_{tn}/ξ_{ti}) translates into the same fractional uncertainty in $(1-\beta_t)$.

For the ratio $\xi_{tn,HiPIMS}/\xi_{tn,dcMS}$, the analysis is more complex. We note that the sputter-rate-normalized deposition rate $F^{IM}_{sput\to IM}$ depends linearly on $(\xi_{tn,HiPIMS}/\xi_{tn,dcMS})^{-1}$ [Eq. (18)]. Therefore, the fractional uncertainty in $\xi_{tn,HiPIMS}/\xi_{tn,dcMS}$ translates into the same fractional uncertainty of $F^{IM}_{sput\to IM}$. The fractional uncertainty of α_t can then be calculated from Eq. (8),

$$\frac{\delta\alpha_t}{\alpha_t} = -\frac{F^{IM}_{sput\to IM}(1-F^{IM}_{ti,flux})}{1-F^{IM}_{sput\to IM}(1-F^{IM}_{ti,flux})}\frac{\delta F^{IM}_{sput\to IM}}{F^{IM}_{sput\to IM}} = c_1\frac{\delta F^{IM}_{sput\to IM}}{F^{IM}_{sput\to IM}}. \quad (A1)$$

For all the discharges investigated here, $|c_1|$ is <0.6, except for the discharge with the weakest magnetic field (C10E10, cf., Table I) for which $|c_1| = 1.2$. A fractional uncertainty in the parameter $\xi_{tn,HiPIMS}/\xi_{tn,dcMS}$, therefore, usually translates into a smaller fractional uncertainty in the parameter α_t.

A similar argument can be made for $(1-\beta_t)$. The fractional uncertainty in $(1-\beta_t)$ is calculated from Eq. (10),

$$\frac{\delta(1-\beta_t)}{(1-\beta_t)} = \frac{1}{1-F^{IM}_{sput\to IM}(1-F^{IM}_{ti,flux})}\frac{\delta F^{IM}_{sput\to IM}}{F^{IM}_{sput\to IM}} = c_2\frac{\delta F^{IM}_{sput\to IM}}{F^{IM}_{sput\to IM}}. \quad (A2)$$

For the discharges investigated here, $|c_2| < 1.6$, except for the discharge with the weakest magnetic field (C10E10, cf., Table I) for which $|c_2| = 2.2$. We note that a fractional uncertainty in $F^{IM}_{sput\to IM}$ can translate into a larger fractional uncertainty of $(1-\beta_t)$.

To conclude, the probability of ionization α_t can be calculated from the model with confidence even if the exact ratios ξ_{tn}/ξ_{ti} and $\xi_{tn,HiPIMS}/\xi_{tn,dcMS}$ are associated with uncertainties. The parameter $(1-\beta_t)$ is associated with a larger uncertainty. The fractional uncertainty of $(1-\beta_t)$ from an uncertain value of ξ_{tn}/ξ_{ti} is equal to the fractional uncertainty of ξ_{tn}/ξ_{ti}. The fractional uncertainty of $(1-\beta_t)$ from an uncertain value of $\xi_{tn,HiPIMS}/\xi_{tn,dcMS}$ is larger than the fractional uncertainty of $\xi_{tn,HiPIMS}/\xi_{tn,dcMS}$, which may lead to large uncertainty bars. There is a need to develop techniques to estimate these transport parameters more precisely. The analysis made here should support the use of the model by providing means to estimate the uncertainty of the derived parameters α_t and β_t.

DATA AVAILABILITY

The data that support the findings of this study are available from the corresponding author upon reasonable request.

REFERENCES

[1]U. Helmersson, M. Lattemann, J. Bohlmark, A. P. Ehiasarian, and J. T. Gudmundsson, "Ionized physical vapor deposition (IPVD): A review of technology and applications," Thin Solid Films **513**, 1–24 (2006).
[2]J. T. Gudmundsson, "Physics and technology of magnetron sputtering discharges," Plasma Sources Sci. Technol. **29**, 113001 (2020).
[3]Z. Hubička, J. T. Gudmundsson, P. Larsson, and D. Lundin, "Hardware and power management for high power impulse magnetron sputtering," in *High Power Impulse Magnetron Sputtering Fundamentals, Technologies, Challenges and Applications*, edited by D. Lundin, T. Minea, and J. T. Gudmundsson (Elsevier, Amsterdam, 2020), pp. 49–80.
[4]M. Samuelsson, D. Lundin, K. Sarakinos, F. Björefors, B. Wälivaara, H. Ljungcrantz, and U. Helmersson, "Influence of ionization degree on film properties when using high power impulse magnetron sputtering," J. Vac. Sci. Technol. A **30**, 031507 (2012).

Published under license by AIP Publishing.

[5]G. Greczynski, I. Petrov, J. E. Greene, and L. Hultman, "Paradigm shift in thin-film growth by magnetron sputtering: From gas-ion to metal-ion irradiation of the growing film," J. Vac. Sci. Technol. A **37**, 060801 (2019).
[6]K. Sarakinos and L. Martinu, "Synthesis of thin films and coatings by high power impulse magnetron sputtering," in *High Power Impulse Magnetron Sputtering Fundamentals, Technologies, Challenges and Applications*, edited by D. Lundin, T. Minea, and J. T. Gudmundsson (Elsevier, Amsterdam, 2020), pp. 333–374.
[7]N. Brenning, A. Butler, H. Hajihoseini, M. Rudolph, M. A. Raadu, J. T. Gudmundsson, T. Minea, and D. Lundin, "Optimization of HiPIMS discharges: The selection of pulse power, pulse length, gas pressure, and magnetic field strength," J. Vac. Sci. Technol. A **38**, 033008 (2020).
[8]N. Brenning, H. Hajihoseini, M. Rudolph, M. A. Raadu, J. T. Gudmundsson, T. Minea, and D. Lundin, "HiPIMS optimization by using mixed high-power and low-power pulsing," Plasma Sources Sci. Technol. (published online).
[9]M. Rudolph, N. Brenning, M. A. Raadu, H. Hajihoseini, J. T. Gudmundsson, A. Anders, and D. Lundin, "Optimizing the deposition rate and ionized flux fraction by tuning the pulse length in high-power impulse magnetron sputtering," Plasma Sources Sci. Technol. **29**, 05LT01 (2020).
[10]J. W. Bradley, A. Mishra, and P. J. Kelly, "The effect of changing the magnetic field strength on HiPIMS deposition rates," J. Phys. D Appl. Phys. **48**, 215202 (2015).
[11]H. Hajihoseini, M. Čada, Z. Hubička, S. Ünaldi, M. A. Raadu, N. Brenning, J. T. Gudmundsson, and D. Lundin, "The effect of magnetic field strength and geometry on the deposition rate and ionized flux fraction in the HiPIMS discharge," Plasma **2**, 201–221 (2019).
[12]T. Kubart, M. Čada, D. Lundin, and Z. Hubička, "Investigation of ionized metal flux fraction in HiPIMS discharges with Ti and Ni targets," Surf. Coat. Technol. **238**, 152–157 (2014).
[13]M. A. Raadu, I. Axnäs, J. T. Gudmundsson, C. Huo, and N. Brenning, "An ionization region model for high-power impulse magnetron sputtering discharges," Plasma Sources Sci. Technol. **20**, 065007 (2011).
[14]C. Huo, D. Lundin, J. T. Gudmundsson, M. A. Raadu, J. W. Bradley, and N. Brenning, "Particle-balance models for pulsed sputtering magnetrons," J. Phys. D Appl. Phys. **50**, 354003 (2017).
[15]N. Britun, M. Palmucci, S. Konstantinidis, and R. Snyders, "Particle visualization in high-power impulse magnetron sputtering. II. Absolute density dynamics," J. Appl. Phys. **117**, 163303 (2015).
[16]A. Butler, N. Brenning, M. A. Raadu, J. T. Gudmundsson, T. Minea, and D. Lundin, "On three different ways to quantify the degree of ionization in sputtering magnetrons," Plasma Sources Sci. Technol. **27**, 105005 (2018).
[17]J. Vlček and K. Burcalová, "A phenomenological equilibrium model applicable to high-power pulsed magnetron sputtering," Plasma Sources Sci. Technol. **19**, 065010 (2010).
[18]J. T. Gudmundsson, N. Brenning, D. Lundin, and U. Helmersson, "High power impulse magnetron sputtering discharge," J. Vac. Sci. Technol. A **30**, 030801 (2012).
[19]D. J. Christie, "Target material pathways model for high power pulsed magnetron sputtering," J. Vac. Sci. Technol. A **23**, 330–335 (2005).
[20]N. Brenning, C. Huo, D. Lundin, M. A. Raadu, C. Vitelaru, G. D. Stancu, T. Minea, and U. Helmersson, "Understanding deposition rate loss in high power impulse magnetron sputtering: I. Ionization-driven electric fields," Plasma Sources Sci. Technol. **21**, 025005 (2012).
[21]N. Britun, M. Palmucci, S. Konstantinidis, and R. Snyders, "Particle visualization in high-power impulse magnetron sputtering. I. 2D density mapping," J. Appl. Phys. **117**, 163302 (2015).
[22]M. A. Lieberman and A. J. Lichtenberg, *Principles of Plasma Discharges and Material Processing*, 2nd ed. (John Wiley & Sons, 2005).
[23]C. Huo, D. Lundin, M. A. Raadu, A. Anders, J. T. Gudmundsson, and N. Brenning, "On sheath energization and ohmic heating in sputtering magnetrons," Plasma Sources Sci. Technol. **22**, 045005 (2013).
[24]N. Brenning, D. Lundin, T. Minea, C. Costin, and C. Vitelaru, "Spokes and charged particle transport in HiPIMS magnetrons," J. Phys. D Appl. Phys. **46**, 084005 (2013).
[25]A. Anders, P. Ni, and A. Rauch, "Drifting localization of ionization runaway: Unraveling the nature of anomalous transport in high power impulse magnetron sputtering," J. Appl. Phys. **111**, 053304 (2012).
[26]A. Anders, M. Panjan, R. Franz, J. Andersson, and P. Ni, "Drifting potential humps in ionization zones: The propeller blades of high power impulse magnetron sputtering," Appl. Phys. Lett. **103**, 144103 (2013).
[27]H. Hajihoseini, M. Čada, Z. Hubička, S. Ünaldi, M. A. Raadu, N. Brenning, J. T. Gudmundsson, and D. Lundin, "Sideways deposition rate and ionized flux fraction in dcMS and HiPIMS," J. Vac. Sci. Technol. A **38**, 033009 (2020).
[28]J. Hopwood, "Ionized physical vapor deposition of integrated circuit interconnects," Phys. Plasmas **5**, 1624–1631 (1998).
[29]C. Huo, D. Lundin, M. A. Raadu, A. Anders, J. T. Gudmundsson, and N. Brenning, "On the road to self-sputtering in high power impulse magnetron sputtering: Particle balance and discharge characteristics," Plasma Sources Sci. Technol. **23**, 025017 (2014).
[30]A. Anders, "Deposition rates of high power impulse magnetron sputtering: Physics and economics," J. Vac. Sci. Technol. A **28**, 783–790 (2010).
[31]C. Huo, M. A. Raadu, D. Lundin, J. T. Gudmundsson, A. Anders, and N. Brenning, "Gas rarefaction and the time evolution of long high-power impulse magnetron sputtering pulses," Plasma Sources Sci. Technol. **21**, 045004 (2012).
[32]C. Vitelaru, D. Lundin, G. D. Stancu, N. Brenning, J. Bretagne, and T. Minea, "Argon metastables in HiPIMS: Time-resolved tunable diode-laser diagnostics," Plasma Sources Sci. Technol. **21**, 025010 (2012).
[33]A. V. Phelps, C. H. Greene, and J. P. Burke, "Collision cross sections for argon atoms with argon atoms for energies from 0. 01 eV to 10 keV," J. Phys. B At. Mol. Opt. Phys. **33**, 2965–2981 (2000).
[34]T. Shimizu, M. Zanáška, R. P. Villoan, N. Brenning, U. Helmersson, and D. Lundin, "Experimental verification of deposition rate increase, with maintained high ionized flux fraction, by shortening the HiPIMS pulse," Plasma Sources Sci. Technol. (submitted).
[35]M. Rudolph, A. Revel, D. Lundin, H. Hajihoseini, N. Brenning, M. A. Raadu, A. Anders, T. Minea, and J. T. Gudmundsson, "On the electron energy distribution function in the high-power impulse magnetron sputtering discharge" (unpublished).

Published under license by AIP Publishing.